Solid-State NMR Investigations of Peptide−Lipid Interaction and Orientation of a β-Sheet Antimicrobial Peptide, Protegrin†

Satoru Yamaguchi,‡ Teresa Hong,§ Alan Waring,§ Robert I. Lehrer,§ and Mei Hong*,‡

Department of Chemistry, Iowa State University, Ames, Iowa 50011, and Department of Medicine, University of California at Los Angeles School of Medicine, Los Angeles, California 90095

Received March 12, 2002; Revised Manuscript Received May 11, 2002

ABSTRACT: Protegrin-1 (PG-1) is a broad-spectrum β-sheet antimicrobial peptide found in porcine leukocytes. The mechanism of action and the orientation of PG-1 in lipid bilayers are here investigated using ^{2}H, ^{31}P, ^{13}C, and ^{15}N solid-state NMR spectroscopy. ^{2}H spectra of mechanically aligned and chain-perdeuterated 1-palmitoyl-2-oleoyl-*sn*-glycero-3-phosphatidylcholine (POPC) bilayers indicate that PG-1 at high concentrations destroys the orientational order of the aligned lamellar bilayer. The conformation of the lipid headgroups in the unoriented region is significantly altered, as seen from the ^{31}P spectra of POPC and the ^{2}H spectra of headgroup-deuterated 1,2-dipalmitoyl-*sn*-glycero-3-phosphatidylcholine. These observations indicate that PG-1 disrupts microbial membranes by breaking the extended bilayer into smaller disks, where a significant fraction of lipids is located in the edges of the disks with a distribution of orientations. These edges allow the lipid bilayer to bend back on itself as in toroidal pores. Interestingly, this loss of bilayer orientation occurs only in long-chain lipids such as POPC and not in shorter chain lipids such as 1,2-dilauroyl-*sn*-glycero-3-phosphatidylcholine (DLPC). To understand the mode of binding of PG-1 to the lipid bilayer, we determined the orientation of PG-1 in DLPC bilayers. The ^{13}CO and ^{15}N chemical shifts of Val-16 labeled PG-1 indicate that the β-strand axis is tilted by 55° ± 5° from the bilayer normal while the normal of the β-sheet plane is 48° ± 5° from the bilayer normal. This orientation favors interaction of the hydrophobic backbone of the peptide with the hydrophobic core of the bilayer and positions the cationic Arg side chains to interact with the anionic phosphate groups. This is the first time that the orientation of a disulfide-stabilized β-sheet membrane peptide has been determined by solid-state NMR.

Antimicrobial peptides are evolutionarily conserved elements of the innate immune system produced by mammals, amphibians, and insects to kill a broad range of pathogens such as bacteria, viruses, and fungi (*1*). In general, they act with high potency and speed by disrupting the cell membranes of the invading organisms. Since microorganisms cannot easily develop resistance to these compounds, antimicrobial peptides provide a promising alternative to conventional antibiotics. However, for many antimicrobial peptides, the structural basis of their antimicrobial action is still incompletely understood.

Antimicrobial peptides share some common structural characteristics. They tend to be short, consisting of 15−45 residues. They are rich in cationic residues Arg and Lys. They are often amphipathic, as manifested by the helical wheel diagrams of helical peptides such as magainin (*2*). Most of these peptides can be sorted into three subclasses according to their predominant conformation: α-helical peptides such as cecropins and melittin; β-sheet peptides such as defensins, protegrins, and tachyplesins; and peptides with mixed conformations or rich in β-turn structures, such as nisin and tritrpticin (*3*).

While structurally diverse, antimicrobial peptides generally kill microbes by disrupting the cell membranes. This conclusion is based on the observation that many all-D-amino acid analogues of these peptides possess the same antibiotic activities as the parent L-enantiomers (*4*, *5*); thus chiral receptors cannot be involved in antimicrobial activities. Specific models of antimicrobial peptide−lipid interaction have been proposed (*6*). The barrel-stave model postulates that a bundle of helical peptides forms a membrane-spanning aqueous pore, thus destroying the membrane potential. The main evidence for this model comes from conductance measurements on alamethicin (*7*−*9*), a mostly hydrophobic peptide. The toroidal or wormhole model postulates that the peptides form a dynamic supramolecular complex with lipids, with the polar faces of the peptides associated with the polar headgroups of the lipids (*2*). In contrast to the barrel-stave model, the lipids in these toroidal openings tilt from the lamellar normal and connect the two leaflets of the membrane. This model is supported by measurements of the lipid flip-flop rate, peptide translocation rate (*2*), and neutron diffraction experiments (*10*). In the carpet model, aggregated helices lie in the plane of the bilayer, due to the favorable electrostatic interaction between the cationic peptide and the

† M.H. acknowledges the Arnold and Mabel Beckman Foundation for a Young Investigator Award and the Sloan Foundation for a Research Fellowship. Support for this study was also provided by Grants AI 22839 and AI-37945 from the National Institutes of Health.

* Corresponding author. E-mail: mhong@iastate.edu. Tel: (515) 294-3521. Fax: (515) 294-0105.

‡ Iowa State University.

§ University of California at Los Angeles School of Medicine.

10.1021/bi0257991 CCC: $22.00
Published on Web 07/16/2002

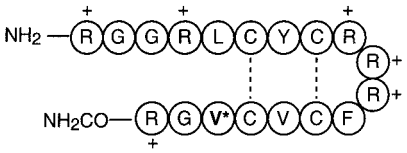

FIGURE 1: Amino acid sequence and structural topology of PG-1. The Arg residues are indicated by their positive charges. The ^{15}N- and ^{13}C-labeled Val-16 is indicated by a star.

anionic lipid headgroups. Membrane permeabilization occurs as a result of micellization as the peptide concentration increases above a threshold value (*11*). This model is supported by solid-state NMR studies of magainins and cecropins (*12*−*14*) and by fluorescence experiments on dermaseptin (*11*) and magainin (*15*).

As this brief survey shows, most models of antimicrobial activity so far are based on linear α-helical peptides. In comparison, knowledge of the mechanism of action of β-sheet peptides is relatively limited (*16*). The only specific β-sheet peptide model available was for human defensin HNP-3, whose crystal structure is known (*17*). There, the observed dimeric structure of HNP-3 was used to suggest that the hydrophobic face of the dimer inserts into the membrane as a wedge or contacts the lipids to form a transmembrane pore.

Protegrin-1 (PG-1,[1] MW 2154 Da) is an 18-residue broad-spectrum antimicrobial peptide found in porcine leukocytes (*18*) (Figure 1). In vitro microbroth dilution assays showed that it is effective against Gram-positive bacteria, Gram-negative bacteria, and fungi (*19*). It also exhibits modest antiviral activities against HIV-1 (*20*), similar to tachyplesin and polyhemusins (*21*). IB-367, a PG-1 analogue, is now in phase III human clinical trials as a topical antibiotic (*22*). In solution, PG-1 forms an antiparallel β-strand connected by a loop (*23*, *24*). The six positively charged Arg residues in the molecule are distributed at the two ends of the long axis of the peptide (Figure 1). This β-hairpin structure is stabilized by two disulfide bonds among four Cys residues. This disulfide bond-stabilized β-sheet conformation is representative of a number of antimicrobial peptides such as human defensins and tachyplesin.

Solid-state NMR spectroscopy has been widely used to study the structure of small insoluble peptides, including those that associate with membranes, form fibrous aggregates, or associate with biomineral surfaces (*25*−*28*). For membrane-bound peptides, solid-state NMR has the ability to probe lipid bilayers and their peptide components directly in the biologically relevant liquid-crystalline state. ^{13}C, ^{15}N, and other isotopic labels can be readily incorporated into these short peptides at sites of interest during solid-phase synthesis. The high degree of control, versatility, and lack of perturbation to the membrane make solid-state NMR an ideal spectroscopic method to study small membrane peptides.

To better understand the mode of action of PG-1 and other analogous β-sheet antimicrobial peptides, we have carried out a solid-state NMR investigation of the protegrin−lipid interactions as a function of peptide concentration and lipid chain length. We also determined the orientation of the peptide in dilauroylphosphatidylcholine by ^{13}C and ^{15}N chemical shift measurements. This demonstrates that solid-state NMR is a valuable approach for characterizing the insertion of β-sheet peptides in membrane ensembles. On the basis of these lipid and peptide results, we propose a mechanism for the antimicrobial action of PG-1.

EXPERIMENTAL PROCEDURES

Materials. All lipids, including 1,2-dilauroyl-*sn*-glycero-3-phosphatidylcholine (DLPC), 1,2-dimyristoyl-*sn*-glycero-3-phosphatidylcholine (DMPC), 1,2-dipalmitoyl-*sn*-glycero-3-phosphatidylcholine (DPPC), 1-palmitoyl-2-oleoyl-*sn*-glycero-3-phosphatidylcholine (POPC), 1-palmitoyl-d_{31}-2-oleoyl-*sn*-glycero-3-phosphatidylcholine (POPC-d_{31}), and 1,2-dipalmitoyl-*sn*-glycero-3-phosphatidylcholine with headgroup deuteration (DPPC-d_{13}), were purchased from Avanti Polar Lipids, Inc. (Alabaster, AL). The main-phase transition temperatures of the lipids are −1 °C for DLPC, 23 °C for DMPC, 41 °C for DPPC, and −2 °C for POPC. Trifluoroethanol (TFE) and chloroform were purchased from Aldrich Chemicals. Cover glasses of 0.06−0.08 mm thickness were purchased from Marienfeld Laboratory Glassware (Germany). ^{15}N-Labeled L-valine and ^{13}C-labeled L-valine were obtained from Cambridge Isotope Laboratories (Andover, MA) and converted to the Fmoc derivative by AnaSpec, Inc. (San Jose, CA).

Peptide Synthesis and Purification. PG-1 was synthesized on a 0.25 mmol scale with a Perkin-Elmer ABI 431A or 433A synthesizer using Fmoc-Rink Amide MBHA resin (AnaSpec, San Jose, CA). A synthesis strategy employing FastMoc chemistry (*29*) and double coupling for all residues was used to optimize the peptide yield. The crude peptide was reduced in a solution with excess dithiothreitol in 6 M guanidine hydrochloride, 0.2 M Tris-HCl, and 0.2 mM EDTA (pH 8.2) under nitrogen at 50 °C for 15 h. At the end of this period, the reaction was terminated by addition of glacial acetic acid to 5 vol %. The crude reduced peptide was then purified by reverse-phase HPLC with a Vydac C18 column (Hesperia, CA). Separation was performed at a flow rate of 10 mL/min employing a linear gradient (0−70% solvent B) of water containing 0.1% TFA (solvent A) and acetonitrile containing 0.1% TFA (solvent B). After this step the reduced peptide appeared homogeneous as measured by MALDI-TOF and analytical reverse-phase HPLC on a Vydac 218TP54 column.

Folding and oxidation of the purified PG-1 were carried out by dissolving the reduced peptide in 0.1% acetic acid at a concentration of 0.1 mg/mL. The pH of the solution was then adjusted to 7.4 with ammonium hydroxide, and the solution was stirred at 25 °C for 24 h. The reaction was terminated by addition of acetic acid to 5%. The oxidized peptide was purified by reverse-phase HPLC under the same conditions as used for the reduced material, and the mass of the oxidized peptide was confirmed by MALDI-TOF mass spectrometry. Previous studies showed that, under these conditions, the synthetic peptide exhibits the same disulfide connectivities as the natural PG-1 (*23*, *30*).

NMR Sample Preparation. Oriented membrane samples were prepared on 12 mm × 6 mm or 16 mm × 4.5 mm

[1] Abbreviations: POPC, 1-palmitoyl-2-oleoyl-*sn*-glycero-3-phosphatidylcholine; DPPC, 1,2-dipalmitoyl-*sn*-glycero-3-phosphatidylcholine; PG-1, protegrin-1; DLPC, 1,2-dilauroyl-*sn*-glycero-3-phosphatidylcholine; DMPC, 1,2-dimyristoyl-*sn*-glycero-3-phosphatidylcholine; TFE, trifluoroethanol.

cover glasses with an average thickness of 73 μm. Each NMR sample typically included 20−30 glass plates. The total peptide amount was about 5 mg for the ^{13}C- and ^{15}N-labeled samples for the chemical shift measurements and about 1 mg for unlabeled samples for the peptide−lipid interaction experiments. The peptide was dissolved in TFE and mixed with chloroform solutions containing the appropriate lipids. The peptide-to-lipid molar ratio (P/L) was adjusted as desired. The mixed solution was deposited onto each cover glass, dried thoroughly in air for 2 days, and then equilibrated for 2 days in a chamber containing a saturated sodium sulfate solution with a constant humidity of 93%. The plates were then stacked and stored at 4 °C in the same humidity until use. Just before the NMR experiment, the stacked glass plates were wrapped in Parafilm and sealed in polyethylene bags to prevent them from drying during the NMR experiment. The degree of hydration using this procedure was measured by FT-IR to be 50% ± 3% water by weight for all membranes except for DPPC (35%) (*31*, *32*). These hydration levels of above 30% correspond to fully hydrated bilayers, similar to that observed before (*33*). The observed ^{2}H quadrupolar splittings of the lipid chains are also consistent with fully hydrated, liquid-crystalline, bilayers.

The unoriented lipid−PG-1 mixtures were prepared by codissolving the peptide and lipids in TFE and chloroform solutions. The solution was dried under a stream of N_2 gas, and the resulting membrane film was redissolved in a small amount of cyclohexane. This was lyophilized and then hydrated to 30−35% water by weight. The sample was frozen in liquid nitrogen to a pellet and transferred to a glass tube. The sample was restricted to the center of the coil to reduce the inhomogeneity of the radio-frequency (rf) field.

Solid-State NMR Spectroscopy. The NMR experiments were carried out on a Bruker DSX-400 spectrometer (Karlsruhe, Germany) operating at a resonance frequency of 400.49 MHz for ^{1}H, 162.12 MHz for ^{31}P, 100.72 MHz for ^{13}C, 61.48 MHz for ^{2}H, and 40.58 MHz for ^{15}N. A high-power static probe with a 5 mm diameter solenoid coil was used for experiments on unoriented powder samples. For the oriented samples, custom-designed rectangular rf coils with the dimension of 16 × 4.5 × 4.5 mm or 12 × 6 × 3.5 mm were used. The coils tuned to all nuclear spin frequencies of interest. Typical ^{15}N, ^{13}C, ^{2}H, and ^{31}P 90° pulse lengths were 6, 5, 3.5, and 4.5 μs, respectively. The rf field strengths for cross-polarization and decoupling were about 45 and 75 kHz, respectively. The cross- polarization contact time was 500 μs for both ^{13}C and ^{15}N experiments. The spectral widths for ^{13}C and ^{15}N experiments were 50 and 40 kHz, respectively. The ^{13}C and ^{15}N spectra were typically averaged over 25000 scans. The recycle delays for ^{15}N and ^{13}C experiments were about 1 s. The ^{2}H spectra were acquired using a quadrupolar echo sequence, with a recycle delay of 0.5 s and a spectral width of 500 kHz. All experiments were carried out well above the gel-to-liquid-crystalline phase transition temperature of the lipids. The ^{15}N chemical shifts were referenced indirectly to liquid ammonia through ^{15}N-labeled ubiquitin. The ^{13}C and ^{31}P chemical shifts were referenced externally to methanol (49.3 ppm) and 85% H_3PO_4 (0 ppm), respectively.

Orientation Calculations. The ^{13}CO and ^{15}N chemical shift frequencies of mechanically aligned PG-1 were calculated as a function of the peptide orientation with respect to the bilayer normal. The Fortran programs written for this purpose take the rigid-limit ^{13}CO and ^{15}N chemical shift principal values and principal axis orientations in the molecular frame as input parameters. For ^{13}CO of Val-16, the rigid-limit principal values were σ_{11} = 244 ppm, σ_{22} = 178 ppm, and σ_{33} = 88 ppm, based on direct measurements on the lyophilized peptide. These values are consistent with the standard ^{13}CO chemical shifts determined in small model peptides (*34*). Note that the isotropic shift of 170 ppm is consistent with the β-sheet conformation. The ^{13}CO σ_{22} axis is parallel to the CO bond, while the σ_{33} axis is normal to the peptide plane. For ^{15}N, literature values of σ_{11} = 217 ppm, σ_{22} = 77 ppm, and σ_{33} = 64 ppm were used (*35*). The σ_{11} axis is 17° from the N−H bond, while the σ_{33} axis is tilted from the peptide plane by 25° (*36*, *37*). The programs calculate the ^{13}CO and ^{15}N chemical shifts of Val-16 in PG-1 as a function of the molecular orientation with respect to the magnetic field. For 0° oriented samples, the bilayer normal is parallel to the magnetic field. Thus, the peptide orientation relative to the field is the same as its orientation relative to the bilayer normal. The peptide in the PDB coordinate frame (PDB accession code: 1PG1) was rotated through all combinations of the polar angle (β) and azimuthal angle (α) that describe the relative orientations between the chemical shift tensors and the magnetic field. The resulting anisotropic ^{13}CO and ^{15}N frequencies were plotted as a function of α and β. The frequencies that agree best with the experimental values yield the orientation of the peptide relative to the bilayer normal.

In these orientation calculations, the α and β angles were incremented in 1° steps, although a step size of 3° yielded nearly identical results. The PDB file of PG-1 contained 20 minimum energy structures. Structure 14, which shows the most regular β-sheet geometry, was chosen in the main chemical shift calculations. Four other structures were also used to repeat the calculations in order to estimate the uncertainties in the orientation result (see Results). The use of the solution structure for determining the orientation of membrane-bound PG-1 is justified, since solution NMR studies of PG-1 in water and in dimethyl sulfoxide showed that there are little conformational differences between the polar solvent and the hydrophobic solvent (*24*). This structural stability is not surprising due to the two disulfide bonds that link the two strands of the β-hairpin peptide. Moreover, a solution NMR structure of PG-1 in DPC micelles concluded that the peptide adopts a similar structure in the micelle as in aqueous solution, except that it aggregates to form dimers. Thus, the use of the solution structure of PG-1 for the membrane-bound peptide is an excellent approximation.

The above approach of calculating the peptide orientation relative to the bilayer normal yields an absolute orientation that is independent of the definition of the β-strand axis and β-sheet plane. Alternatively, we can also calculate the chemical shifts by first defining a β-strand axis on the basis of the average CO−N bond directions for several consecutive residues and varying the orientation of this β-strand axis. However, the peptide has a nonnegligible curvature; thus the definition of the β-strand axis is somewhat arbitrary. This gave rise to apparently different values of the peptide tilt angle. The approach of calculating the orientation of the Val-16 ^{13}CO and ^{15}N chemical shifts directly with respect to the

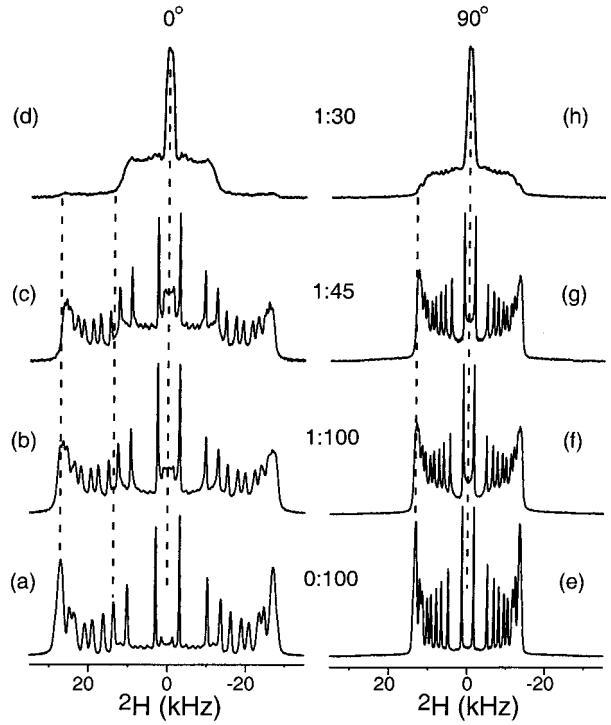

FIGURE 2: ^{2}H spectra of oriented POPC-d_{31} with varying concentrations of PG-1. The samples were oriented with the bilayer normal parallel (a−d) and perpendicular (e−h) to the magnetic field. P/L ratios are (a, e) 0:100, (b, f) 1:100, (c, g) 1:45, and (d, h) 1:30. The spectra were acquired at 293 K. A total of 3000−6000 scans were coadded for each spectrum.

magnetic field circumvents this problem. Moreover, it provides a convenient way of visualizing the peptide. The best-fit orientation angles (α, β) define the direction of the bilayer normal as the line connecting the origin (0, 0, 0) and the point (x, y, z) = (cos α sin β, sin α sin β, cos β). These two points were added to the PDB coordinates of PG-1 and visualized using the Biopolymer module of the INSIGHT II program on a Silicon Graphics workstation. The bilayer normal was made vertical and parallel to the plane of the screen. Rotation around this axis gave various views of the peptide. The tilt angle, τ, of the β-strand axis was determined from the view with the maximal visual tilt from the bilayer normal. To describe the orientation of the β-sheet plane, we define a rotation angle, ϕ, between the bilayer normal ($\vec{n}$) and the normal to the β-sheet plane. This angle is related to the tilt angle τ and the azimuthal angle, ρ, of the β-sheet plane according to cos ϕ = sin τ sin ρ. To determine the azimuthal angle ρ, we first define the x-axis of the β-sheet plane, $\vec{x}_{strand}$, as the average of the C−O and N−H vectors of the rigid central part of the peptide. This is perpendicular to the β-strand axis, $\vec{z}_{strand}$. Once the bilayer normal $\vec{n}$ and the tilt angle τ are determined from the procedure described above, then ρ is determined from the relation $\vec{n}\cdot\vec{z}_{strand}$ = sin τ cos ρ.

RESULTS

Concentration Dependence of PG-1−POPC Interactions. To understand how PG-1 affects the structure and dynamics of lipid bilayers, we examined the ^{2}H and ^{31}P spectra of POPC bilayers containing varying amounts of the peptide. Figure 2 shows the ^{2}H spectra of oriented POPC-d_{31} membranes for P/L ratios from 0 to 1:30. The samples were oriented with the glass plate normal alternately parallel (0°, left column) and perpendicular (90°, right column) to the external magnetic field. For the 0° orientation, in the absence of PG-1, the lipids exhibit resolved splittings with quadrupolar couplings ranging from 26.6 to 3.0 kHz. These quadrupolar splittings are characteristic of the varying dynamic disorder of the CD_2 groups along the lipid acyl chains. The order parameters, which are proportional to the observed splittings, are largest for sites closer to the glycerol backbone and decrease down the acyl chain toward the center of the bilayer (*33*, *38*, *39*).

When PG-1 was added to POPC at P/L =1:100, the ^{2}H spectrum shows several changes. The line widths increased, and below the sharp splittings, a broad background signal from unoriented lipids is observed. The quadrupolar splittings decreased slightly. Moreover, growing intensities at the center of the spectrum were detected. This trend became more prominent as the peptide concentration increased to 1:45. Then, at P/L = 1:30, the spectrum changed dramatically: all resolved splittings disappeared, replaced by a powder-like line shape dominated by a strong zero-frequency peak.

Although the ^{2}H quadrupolar splittings in the 0° oriented 1:30 spectrum (Figure 2d) appear almost a factor of 2 smaller than the lower concentration spectra, a careful inspection indicates that the coupling reduction is actually much less. The apparent difference results from the fact that, in a ^{2}H powder spectrum, the maximum intensity comes from those molecules whose C−D bonds are oriented perpendicular (90°) to the magnetic field. This 90° frequency is exactly half the size of the maximum splitting, which corresponds to the 0° orientation of the C−D bond from the magnetic field. The intensity of the 0° frequency edge is low, since the number of molecules with this orientation is small in an isotropic powder. In contrast, in a uniaxially aligned lipid sample with the alignment axis parallel to the magnetic field, all C−D bonds yield intensities at the 0° frequency position. Thus, the 0° oriented spectrum shows maximum intensities at twice the quadrupolar splittings of the powder spectra.

To confirm that the lipid chain ^{2}H quadrupolar couplings are not strongly attenuated at P/L = 1:30, we measured the ^{2}H spectra with the glass plate normal perpendicular to the magnetic field. At this 90° orientation, the oriented spectra exhibit intensities only at the 90° frequency, the same as that of the maximum intensities in the powder spectra. Figure 2e−h display the series of 90° oriented POPC spectra with P/L from 0 to 1:30. Indeed, the powder spectrum (Figure 2h) shows approximately the same, not much smaller, maximum splitting as that of the oriented spectra. Therefore, the lipid chain order parameters are largely unperturbed by PG-1.

To determine the cause for the increased ^{2}H line widths at high PG-1 concentrations, we compared the ^{2}H transverse relaxation times (T_2) at two P/L ratios, 1:100 and 1:30. Figure 3 shows representative spectra of the 90° samples and the normalized intensities, plotted on a logarithmic scale, as a function of the quadrupolar-echo delay time. At P/L = 1:30, the T_2 of the largest CD_2 splitting is 402 ± 38 μs, a roughly 2.5-fold reduction from 944 ± 47 μs at P/L = 1:100. For the CD_3 group at the center of the spectra, the T_2 is 605 ± 22 μs at P/L = 1:30 but a much longer 1329 ± 119 μs at P/L = 1:100.

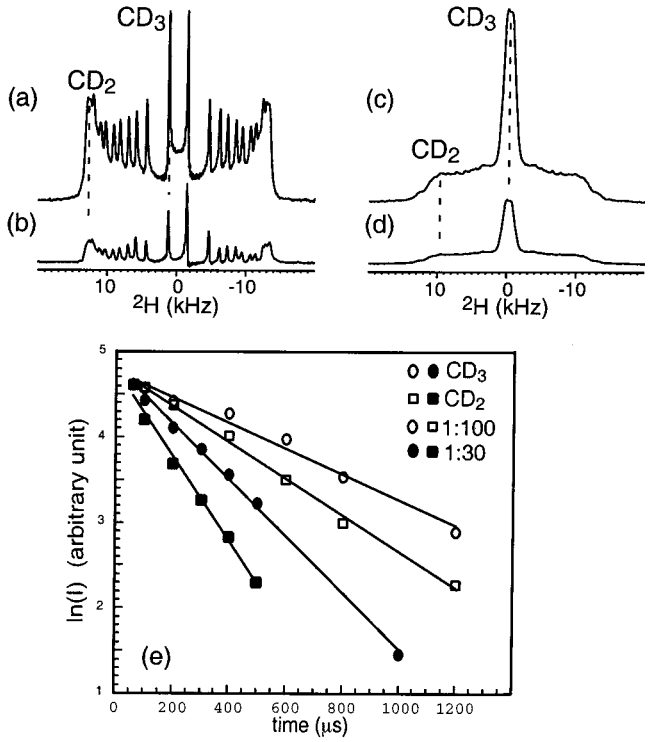

FIGURE 3: ^{2}H T_2 relaxation times of oriented POPC-d_{31} with (a, b) P/L = 1:100 and (c, d) P/L = 1:30. The delay time for the quadrupolar echo was (a) 60 μs, (b) 800 μs, (c) 60 μs, and (d) 500 μs. (e) Logarithmic intensity as a function of echo delay time for the CD_3 signal (circles) and the CD_2 signal (squares) with the largest quadrupolar splitting. Filled symbols: P/L = 1:30. Open symbols: P/L = 1:100.

While ^{2}H NMR of chain-perdeuterated POPC probes the structure and dynamics of the hydrophobic part of the lipid bilayer, ^{31}P NMR provides information on the lipid headgroup in the presence of PG-1. Figure 4 shows the ^{31}P spectra of 0° oriented (left column) and 90° oriented (right column) POPC with P/L from 0 to 1:20. Similar to the ^{2}H spectra, the relative intensities of unoriented lipids increased with PG-1 concentration. For example, without the peptide, more than 80% of the spectral intensity is concentrated in the 0° frequency peak at 31 ppm (Figure 4a), indicating that most lipids are aligned with their bilayer normal parallel to the magnetic field. In comparison, at P/L = 1:45, only about 45% of the intensity is located at this frequency. The rest is distributed over a range of frequencies, especially at the 90° frequency (−13.7 ppm). Above P/L = 1:30, the ^{31}P spectra changed drastically. For the 0° oriented sample (Figure 4c), the 31 ppm peak disappeared completely, while an amorphous pattern from about 10 to −15 ppm is observed. This line shape is distinctly different from the classical spectrum of unoriented Lα-phase lipids. Comparison between the parallel-oriented sample (Figure 4c) and the perpendicular-oriented sample (Figure 4g) indicates that the overall anisotropic span of the ^{31}P spectrum at P/L = 1:30 decreased to about 55% of the span of the normal bilayer, which is 49 ppm. As P/L increased to 1:20, a reversal of the sign of the 0° frequency and the 90° frequency is also observed. For normal Lα-phase lipids, the 0° frequency is downfield from the 90° frequency (Figure 4a,e), while the PG-1-bound POPC shows 0° frequencies upfield from the 90° frequencies (Figure 4d,h).

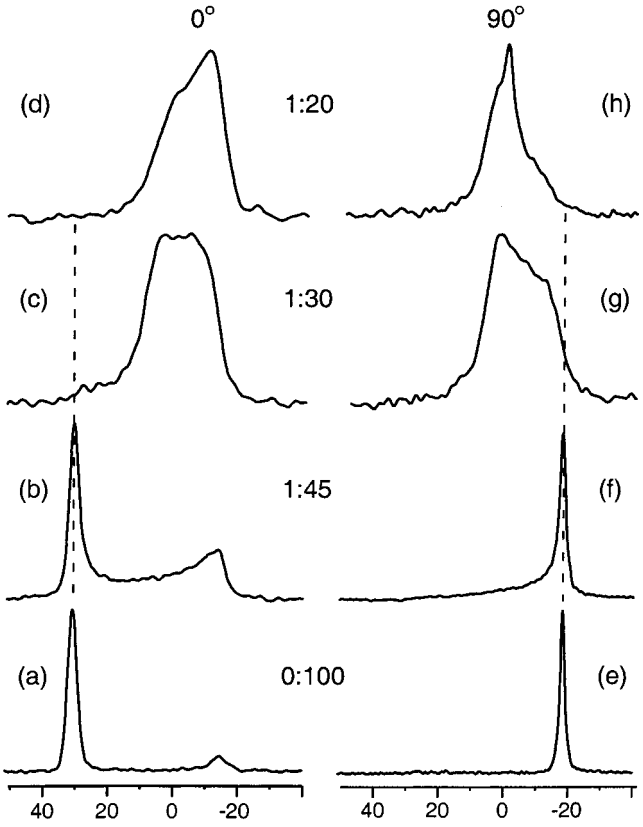

FIGURE 4: ^{31}P spectra of oriented POPC with varying concentrations of PG-1. The glass plate normal is alternately parallel (a−d) and perpendicular (e−h) to the magnetic field. P/L ratios are (a, e) 0:100, (b, f) 1:45, (c, g) 1:30, and (d, h) 1:20.

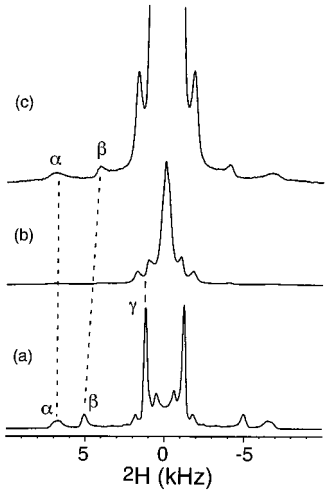

FIGURE 5: ^{2}H spectra of headgroup-deuterated DPPC-d_{13} oriented on glass plates (a) without PG-1 and (b) with PG-1 at P/L = 1:20. (c) Expansion of (b) to show the quadrupolar splittings of the α- and β-CD_2 groups. The assignment of spectrum c was based on 2D ^{13}C−^{1}H dipolar coupling measurements.

The lipid headgroup conformation as probed from the ^{31}P spectra can be altered both by the packing and orientation of the lipid molecules and by membrane surface charges introduced by ions or peptides. To probe the phosphocholine headgroup conformation in more detail, we acquired the ^{2}H spectra of headgroup-deuterated DPPC-d_{13} without (Figure 5a) and with (Figure 5b,c) PG-1. We focus on the large splittings that result from lipids in the oriented region of the bilayer and neglect the central part of the spectrum, which

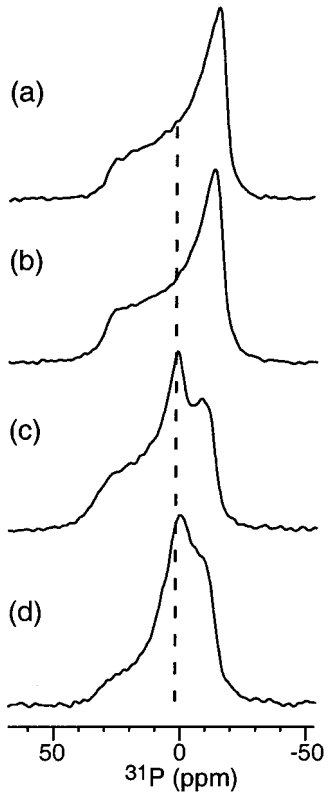

FIGURE 6: ^{31}P powder spectra of PG-1-bound phosphocholine with varying chain lengths: (a) DLPC, $T = 293$ K; (b) DMPC, $T = 303$ K; (c) DPPC, $T = 318$ K; (d) POPC, $T = 293$ K. The P/L ratio is 1:20 for all samples.

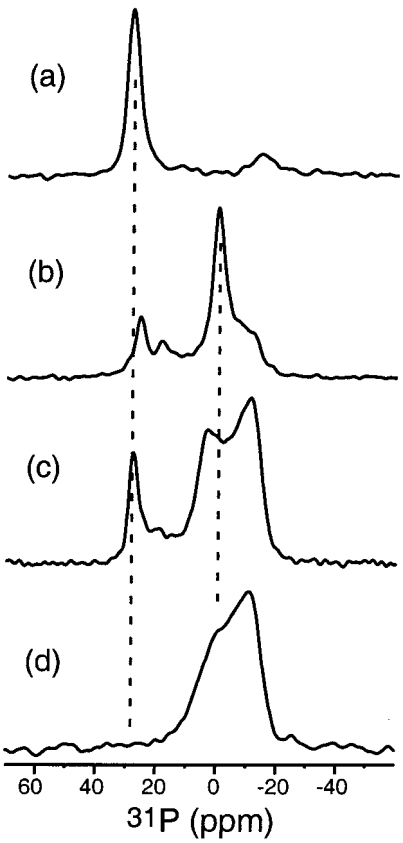

FIGURE 7: ^{31}P spectra of oriented phosphocholine with varying chain lengths: (a) DLPC, $T = 293$ K; (b) DMPC, $T = 303$ K; (c) DPPC, $T = 322$ K; (d) POPC, $T = 293$ K. The P/L ratio is 1:20 for all samples.

results from unoriented lipids. It can be seen that the ^{2}H splittings were changed by the addition of the peptide. In pure DPPC bilayers, the two splittings, 13.2 and 10 kHz, can be assigned to the α and β CD_2 groups on the basis of the literature (*40*). At P/L = 1:20, the two splittings changed to 13.7 and 8.1 kHz. To assign the two couplings, we carried out 2D magic-angle spinning experiments correlating the ^{13}C−^{1}H dipolar couplings with the ^{13}C isotropic chemical shift (*41*). The ^{13}C−^{1}H dipolar couplings have the same order parameters, S_{CH}, as the ^{2}H quadrupolar couplings. Thus, their correlation with the ^{13}C isotropic shift assigns the β and α C−H couplings unambiguously. The addition of PG-1 was found to decrease the β C−H coupling while leaving the α C−H couplings almost unchanged (spectra not shown). In other words, peptide binding decreased the β S_{CH} while only slightly increasing the C−H quadrupolar couplings of the α segment.

Chain-Length Dependence of PG-1−Membrane Interactions. So far, the protegrin−lipid interaction was examined in POPC lipids, which contain 16−18 carbons in the acyl chains and which are the dominant fatty acid chain lengths in bacterial membranes (*42*). While the results clearly indicate that the lipid bilayer orientational order is disrupted by PG-1, the peptide orientation with respect to the lipid bilayers is still unknown. Since uniaxial membrane alignment is important for measuring the peptide orientation, we investigated whether other lipids can accommodate PG-1 without losing their macroscopic alignment. Figure 6 shows the ^{31}P powder spectra of four phosphocholine lipids, where the acyl chains increase from 12 carbons (DLPC) to a mixture of 16 and 18 carbons (POPC). All samples contain PG-1 at P/L = 1:20. The spectra were acquired at temperatures sufficiently above the main-phase transition temperature of each lipid to ensure that the peptide is in the liquid-crystalline state of the membrane. The shortest lipid, DLPC, showed a virtually identical ^{31}P spectrum as pure lipids. The chemical shift pattern has an asymmetry parameter (η) of 0 and an anisotropic span of 47 ppm. In contrast, the longest lipid, POPC, shows a ^{31}P spectrum noticeably distorted from the $\eta = 0$ line shape: the intensities around 0 ppm increased significantly, while the downfield edge of the spectrum at 30 ppm decreased. This indicates that PG-1 is compatible with thinner bilayers but perturbs the orientation of thicker bilayers. This observation is confirmed by the corresponding ^{31}P spectra of oriented lipids (Figure 7). Protegrin-containing DLPC showed a well-aligned ^{31}P spectrum, while the other lipids showed predominantly unoriented ^{31}P spectra. Since all membrane samples were fully hydrated as determined by FT-IR, these ^{31}P spectral differences reflect true protegrin-induced orientational differences.

Orientation and Dynamics of PG-1 in DLPC Bilayers. Since PG-1 is well aligned in DLPC bilayers at high P/L values, we measured the orientation of the peptide in DLPC by ^{13}C and ^{15}N NMR. These experiments were conducted on Val-16 labeled peptides, where the labels are either ^{13}CO or amide ^{15}N. Val-16 was chosen because it is located in the rigid β-strand region of the peptide, away from both the β-turn and the termini.

In contrast to α-helical membrane peptides, where ^{15}N NMR is sufficient to yield the helix axis orientation, ^{15}N NMR alone is insufficient for extracting the orientation of a

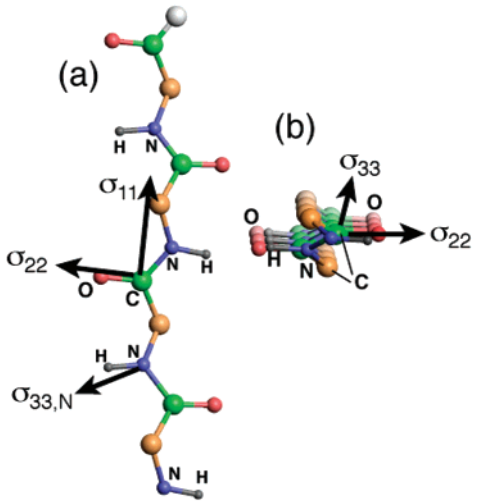

FIGURE 8: ^{13}CO chemical shift tensor orientation in an ideal β-strand peptide. The σ_{22} axis is parallel to the CO bond, the σ_{11} axis is in the peptide plane, roughly along the β-strand axis, and the σ_{33} axis is perpendicular to the peptide plane. (a) View parallel to the β-sheet plane. (b) View perpendicular to the β-sheet plane.

β-sheet peptide in the lipid bilayer. The complexity arises from the fact that the N−H bonds in β-sheets are perpendicular to the strand axis rather than parallel to it. For example, a transmembrane β-sheet peptide and an in-plane β-sheet peptide can both have their ^{15}N−^{1}H bonds perpendicular to the magnetic field and, thus, would be indistinguishable in terms of the NMR frequencies. Only when the β-sheet plane is parallel to the bilayer normal while the β-strand axis is perpendicular to it will the N−H bonds approach the 0° angle relative to the magnetic field. To describe a β-sheet peptide orientation, one needs to specify both the strand axis direction and the β-sheet plane orientation. This requires that the ^{15}N chemical shift be combined with other nuclear spin properties to determine the complete orientation of the peptide.

The carbonyl ^{13}C chemical shift tensor provides an excellent probe of the β-strand axis and β-sheet plane orientations. Various studies of model peptides indicate that the carbonyl carbons typically have chemical shift principal values of σ_{11} = 245 ppm, σ_{22} = 175 ppm, and σ_{33} = 90 ppm (*34*, *43*, *44*). The experimentally measured ^{13}CO principal values of Val-16 in PG-1 agree with these within 3 ppm. In terms of the chemical shift tensor orientation, the σ_{11} axis (245 ppm) points roughly along the β-strand axis, the σ_{22} axis (175 ppm) is parallel to the CO bond in the peptide plane, while the σ_{33} axis (90 ppm) is normal to the peptide plane (*34*, *45*). This is shown in Figure 8 for an ideal β-strand peptide.

Figure 9 shows the ^{13}C spectra of Val-16 ^{13}CO-labeled PG-1. The peptide was oriented in DLPC bilayers with the glass plate normal alternately parallel (a, b) and perpendicular (c, d) to the magnetic field. To distinguish the natural abundance CO signals of the lipids from the Val-16 CO signal, we acquired the ^{13}C spectra of DLPC without the peptide. The comparison between the two spectra shows that the Val-16 ^{13}CO spin resonates at 216 ± 5 ppm at the parallel orientation and 149 ± 3.5 ppm at the perpendicular orientation.

The ^{15}N spectra of Val-16 ^{15}N-labeled PG-1 in DLPC are shown in Figure 10. When the sample is oriented parallel to

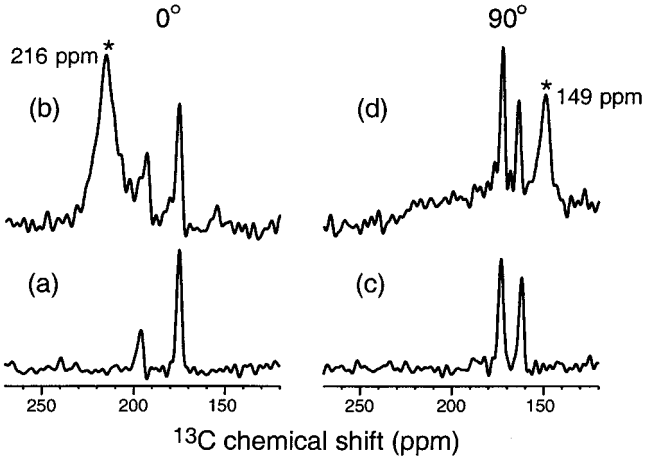

FIGURE 9: Carbonyl region of the ^{13}C spectra of oriented DLPC (a, c) without PG-1 and (b, d) with PG-1 at 1:20 molar ratio. The glass plates were oriented with their normals (a, b) parallel and (c, d) perpendicular to the magnetic field.

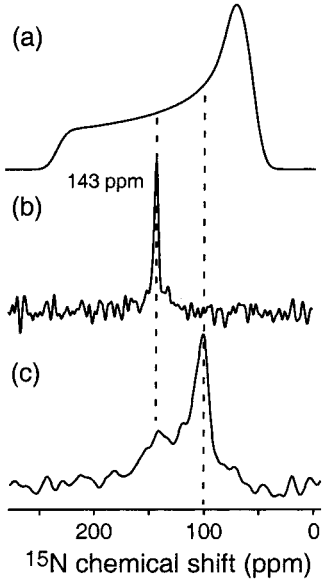

FIGURE 10: (a) Calculated rigid-limit ^{15}N powder spectrum of the amide ^{15}N of peptides. (b) ^{15}N spectrum of V16-labeled PG-1 in oriented DLPC bilayers. P/L = 1:30. The glass plate normal is parallel to the magnetic field. (c) ^{15}N spectrum of V16-labeled PG-1 in unoriented DLPC.

the magnetic field, a sharp signal at 143 ± 2 ppm is observed (Figure 10b). This chemical shift is intermediate between the rigid-limit 0° frequency (217 ppm) and 90° frequency (64 ppm) for a typical peptide amide group (Figure 10a), indicating that the β-strand axis of PG-1 deviates significantly from the bilayer normal. Moreover, since the ^{15}N isotropic shifts in peptides are about 120 ppm, the observed anisotropic shift of 143 ppm suggests that the Val-16 N−H bond is tilted by less than 54.7° from the bilayer normal. Figure 10c shows the ^{15}N powder spectrum of the peptide. A uniaxial powder pattern with reduced chemical shift range is observed, indicating that PG-1 is uniaxially mobile around the bilayer normal. Moreover, since the ^{15}N line shape has the same sidedness as the rigid-limit pattern, the motional order parameter is positive. This is consistent with the observation that the Val-16 N−H bond forms an angle less than 54.7° from the bilayer normal.

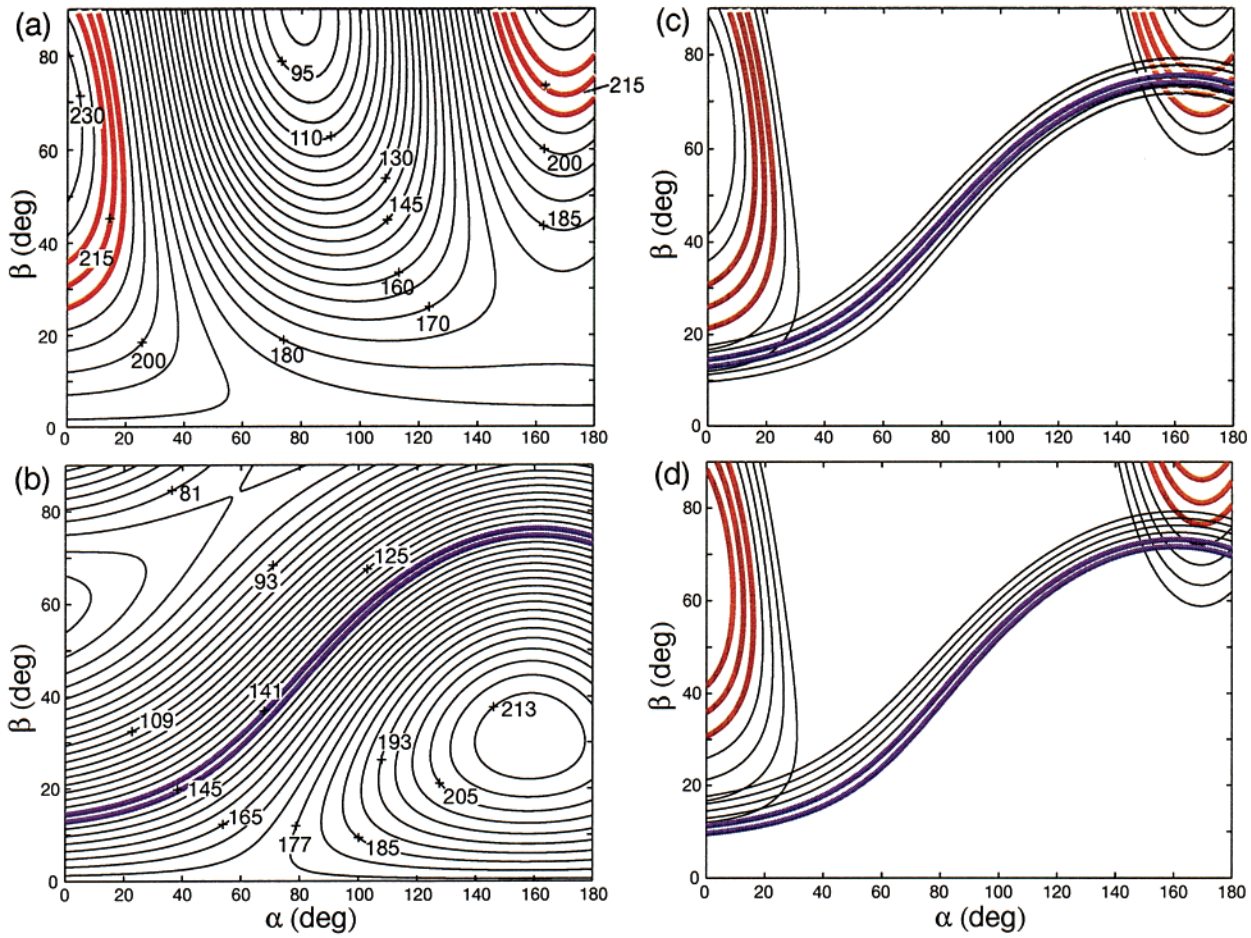

FIGURE 11: Calculated anisotropic chemical shifts of Val-16 in PG-1 as a function of the polar angle β and azimuthal angle α that relates the molecule-fixed PDB frame with the magnetic field or bilayer normal. (a) ^{13}CO chemical shifts, plotted at 5 ppm increments. The contour lines agreeing with the experimental chemical shift of 216 ± 5 ppm are in bold. (b) ^{15}N chemical shifts, plotted at 4 ppm increments. The contour lines agreeing with the experimental chemical shift of 143 ± 2 ppm are in bold. (c) Overlap between the best fit ^{13}CO and ^{15}N chemical shifts. A single solution of α = 170° ± 10° and β = 76° ± 2° is found. (d) ^{13}CO and ^{15}N chemical shifts if a molecular order parameter of 0.95 is assumed. There are no overlapping orientation solutions.

Using the Val-16 ^{13}CO and ^{15}N chemical shifts at the 0° alignment, we calculated the orientation of PG-1 in DLPC bilayers. The calculation is based on the solution structure of PG-1 (*23*) and the experimental ^{13}CO and standard ^{15}N chemical shift tensors. The orientation of the magnetic field, which is identical to the orientation of the bilayer normal in the 0° oriented samples, is rotated through various polar (β) and azimuthal (α) angles with respect to the chemical shift principal axis system. Since the ^{13}C and ^{15}N chemical shift tensors are fixed in the molecule, this yields the frequencies corresponding to different peptide orientations relative to the bilayer normal. Figure 11 shows the calculated ^{13}CO and ^{15}N chemical shifts of oriented PG-1 as a function of the polar coordinates α and β. As usual, for symmetry reasons, β is unique in the 0° to 90° range while α is unique within 0° to 180°. For ^{13}CO chemical shifts, the experimentally measured chemical shift of 216 ± 5 ppm occurs in two regions of the angular plot, one at α angles of ∼20° and the other at large β angles of ∼75° and α angles of about 170°. The experimental ^{15}N chemical shift is found for angles across the entire α, β diagram. While each chemical shift gave multiple orientation solutions, the overlap between the two yielded only a single solution in a very narrow region of the angular space, at α = 170° ± 10°, β = 76° ± 2°.

These polar coordinates define the orientation of the bilayer normal in a molecule-fixed frame intrinsic to the PDB structure. To express this orientation in terms of the tilt angle τ of the β-strand axis and the rotation angle ϕ of the β-sheet plane, we added the bilayer normal coordinates to the PDB structure and set the bilayer normal vertically. Under this condition, the peptide shows a tilt angle of τ = 55° ± 5° and an azimuthal angle of ρ = 125° ± 5° (Figure 12). The angle uncertainty of ±5° takes into account the precision of the frequency measurement and the slight curvature of the peptide backbone. These tilt and azimuthal angles can be converted to the more visual rotation angle, which is 48° ± 5° between the normal of the β-sheet plane and the bilayer normal (Figure 12).

This orientation was obtained by using the most regular structure (structure 14) of PG-1 from the Protein Data Bank. It is interesting to consider how variations among the 20 minimum energy structures affect the angular result. Analysis of the experimental ^{13}CO and ^{15}N chemical shifts using four other structures yielded β-strand tilt angles from 50° to 73°. Therefore, the variations of PG-1 solution structures contribute to a larger uncertainty in the peptide orientation than any solid-state NMR experimental errors. However, it is important to realize that the most divergent orientations also

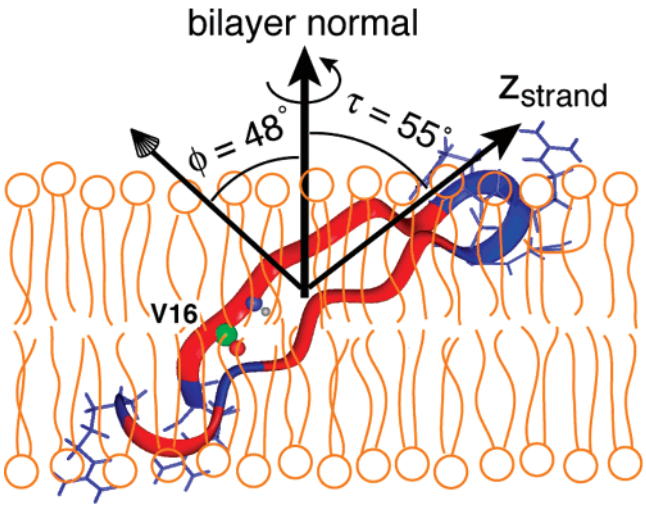

FIGURE 12: Orientation of PG-1 in DLPC bilayers. The β-strand axis is tilted by about 55° from the bilayer normal while the β-sheet plane is rotated by about 48° from the bilayer normal. The labeled Val-16 CO and NH groups are indicated as spheres. The Arg side chains at two ends of the molecule are shown as sticks.

result from the most distorted structure in which the two β-strands of the hairpin are poorly aligned with each other. Since membrane-active peptides are known to adopt more ordered structures in the lipid bilayer than in aqueous or organic solutions, as shown, for example, by the study of PG-1 in DPC micelles (*46*), PG-1 will most likely adopt a more regular β-hairpin structure in the lipid bilayer than in solution. This should reduce the true spread of the tilt angle and the β-sheet plane rotation angle in the membrane to well within 10°.

DISCUSSION

The ^{2}H spectra of POPC-d_{31} show increased line widths, a broad baseline, and a growing zero-frequency peak with increasing PG-1 concentration (Figure 2). These observations indicate that PG-1 induces lipids to adopt chain orientations different from the lamellar region of the bilayer. We interpret these unoriented lipids as located at the edges of lamellar sheets, thus capping and interrupting the bilayer. The headgroups of the lipids in the edges face outward, while their acyl chains are directed toward the interior of the bilayer. As the PG-1 concentration increases further, the size of the lamellar region decreases while the size of the edge region increases, making the stacking of bilayers less favorable. Above a critical concentration, which is between 1:45 and 1:30 for POPC, these bilayer disks become so small that their alignment is almost completely abolished, and the sample approaches a near isotropic orientation distribution. This is demonstrated by the remarkably similar ^{2}H spectra at P/L = 1:30 between the 0° and 90° spectra (Figure 2d,h). Note that the ^{2}H quadrupolar splittings at high PG-1 concentrations are not significantly attenuated but have strengths comparable to those of the oriented lipids. This means that the fragmented lipid disks are not isotropic micelles but are similarly rigid as the regular lipid bilayer. Therefore, only the orientational order, and not the dynamic order, of the lipids is disrupted by PG-1.

In principle, the zero-frequency intensity in the ^{2}H spectra can result either from acyl chains whose chain-end CD_3 groups are nearly isotropically mobile or from a small fraction of lipids that form isotropic micelles due to the action of PG-1. However, micelle formation is unlikely, since the ^{31}P spectra of the same samples (Figure 4) do not exhibit sharp signals at the isotropic chemical shift. Thus, the mobile acyl chain termini most likely account for the broad zero-frequency peak in the ^{2}H spectra.

The ^{2}H T_2 relaxation experiment reports the fraction of lipids that have changed their orientations or frequencies during the delay time between the two 90° pulses and thus did not refocus their intensities into a full echo. The shorter T_2 relaxation times at higher PG-1 concentrations are consistent with the fragmented lipid disk model described above. As the lamellar area decreases with increasing PG-1, the lateral diffusion of the lipids changes the molecular orientations more rapidly than before, from being aligned with the glass plate normal to being tilted. When this orientational change occurs on a time scale comparable to the delays between the ^{2}H pulses, it changes the ^{2}H frequency, thus preventing the refocusing of the ^{2}H signals. This translation-induced orientational change is much slower than the uniaxial rotational diffusion of the lipids around the local bilayer normal; thus it leaves the ^{2}H quadrupolar couplings largely unchanged. Using an average T_2 time of about 500 μs for high concentrations of PG-1 and a lipid translational diffusion coefficient of 10^{-8} cm^2/s (*47*), we estimate that the radius of the fragment lipid disks is about 25 nm.

The ^{31}P spectra of POPC lipids further corroborate the disk theory for protegrin−membrane interactions. The anomalous ^{31}P line shapes at P/L greater than 1:30 reflect the altered conformation of the lipid headgroups in the unoriented edges of the lipid disks. It is well-known that the ^{31}P NMR spectra depend on the lipid phase, the average conformation of the headgroups, and the motion of the molecules (*48*−*50*). Since the ^{31}P spectra at P/L above 1:30 do not correspond to any specific lipid phases, such as Lα, isotropic, and hexagonal phases, it is unlikely that the formation of alternative lipid phases is a cause for the anomalous line shapes. Instead, since the lipids in the unoriented region would have much looser packing for their headgroups than lipids in the lamellar region, and probably interact preferentially with a high concentration of the cationic PG-1, the headgroup conformation must be significantly altered, causing the ^{31}P line shape to change. It is not possible to calculate the ^{31}P spectra of the edge lipids on the basis of these data, since, in general, far more NMR couplings need to be measured to restrain the order tensor of the phosphate headgroup (*51*−*53*).

The ^{2}H spectra of the headgroup-deuterated DPPC in the presence and absence of PG-1 confirm that the cationic peptide affects the conformation of the lipid headgroup. The α-CD_2 quadrupolar splitting increased slightly while the β-CD_2 coupling decreased by about 20%. It is well-known that membrane surface electrostatic charges change the average headgroup conformation and thus the ^{2}H order parameters (*54*−*57*). Previous studies of site-specifically headgroup-deuterated lipids interacting with cationic peptides found the ^{2}Hα quadrupolar coupling to remain unchanged while the ^{2}Hβ coupling to decrease (*58*, *59*). The PG-1 induced changes in the headgroup ^{2}H quadrupolar couplings exhibit a similar trend. To quantify these changes, more detailed knowledge of the depth and the orientation of insertion of PG-1 in POPC is required.

^{31}P spectra of PG-1-bound phosphocholine lipids (Figures 6 and 7) with varying acyl chain lengths indicate that only the long-chain lipids lose their orientational order by PG-1. For the thinnest bilayer examined, DLPC, the addition of peptide did not cause any disruption of the lamellar orientation. The distribution of the positively charged Arg residues in PG-1 suggests a reason for this chain-length dependence. The six Arg residues in PG-1 are clustered at the two ends of the molecule, in the β-turn region and at the N- and C-termini. Sandwiched between these two cationic regions is a stretch of hydrophobic residues containing Val, Leu, Cys, Gly, and the aromatic residues Tyr and Phe (Figure 1). This longitudinal amphiphilicity favors interaction of the central portion of the peptide with the hydrophobic part of the lipid bilayer, and of the two ends of the peptide with the zwitterionic lipid headgroups. If the two hydrophobic lengths match, then the peptide may be incorporated into the bilayer without distorting the lipid structure.

The orientation of PG-1 in DLPC determined from the ^{13}CO and ^{15}N chemical shifts of Val-16 support the importance of hydrophobic matching. The data indicate that the β-strand axis is tilted by 55° from the bilayer normal, while the β-sheet plane is rotated by 48° from the bilayer normal. PG-1 has a backbone length of about 30 Å based on the solution NMR structure (*23*, *24*). Tilted at 55°, the vertical distance of the peptide is about 17 Å. On the other hand, the hydrophobic thickness of the DLPC bilayer is about 20 Å (*60*). Thus, PG-1 is just about sufficient to pass the DLPC bilayer. At the same time, the long cationic Arg side chains protruding out of the two ends of the peptide can interact with the anionic phosphate headgroups of the lipids. The favorable hydrophobic matching and electrostatic attraction should stabilize the orientation of PG-1 in DLPC bilayers.

As observed in other small membrane peptides, the β-sheet PG-1 rotates uniaxially around the bilayer normal when embedded in DLPC bilayers. This is manifested in the reduced ^{13}CO chemical shift difference between the 0° and 90° oriented spectra. The rigid-limit ^{13}CO chemical shift anisotropic span, $\Delta\sigma = \sigma_{11} - \sigma_{33}$, is 156 ppm for Val-16, while the observed chemical shift span is only about 67 ppm. Moreover, since a single sharp peak rather than a distribution of frequencies is observed in the 90° oriented ^{13}CO spectrum, the motion must be uniaxial around the bilayer normal. Any other motional axis would yield a residual frequency distribution, which is not observed here. This motion is confirmed by the reduced chemical shift range of the ^{15}N powder spectrum (Figure 10c). The rotational diffusion must occur at a rate faster than $\sim 10^5$ s^{-1} to average the ^{13}CO and ^{15}N chemical shift interactions.

It is important to consider how motion influences the orientation determination of PG-1. Global reorientation of the peptide around the bilayer normal does not change the chemical shift frequencies as long as the bilayer normal is aligned parallel to the external magnetic field. This is the sample geometry used to obtain the ^{13}CO and ^{15}N chemical shift frequencies inputted into the orientation calculation. Further, the tilt and rotation angles of the β-sheet peptide extracted from the chemical shifts are both invariant under uniaxial motion around the bilayer normal.

The only motions that could affect the orientation determination are internal segmental dynamics of the peptide. Overall, such internal motions are unlikely for PG-1, since the peptide structure is severely restricted by the disulfide bonds that link the two strands of the β-hairpin. Moreover, if we assume an isotropic rotational model with an order parameter of 0.95 and recalculate the peptide orientation, we find no angular solution that satisfies both the ^{13}CO and ^{15}N experimental chemical shifts. At this order parameter of 0.95, the unscaled ^{13}CO and ^{15}N chemical shifts at the 0° sample alignment would be 227 and 150 ppm, respectively. An examination of the chemical shift contour plots (Figure 11d) shows immediately that these two values do not yield any overlapping orientation angles. Smaller order parameters will make the divergence even more severe. In fact, in order for there to be a solution to the peptide orientation, the molecular order parameter must be greater than 0.97. This provides strong evidence that PG-1 has very little internal motion. It also confirms that there is only one well-defined orientation for the β-hairpin PG-1 in DLPC lipids.

On the basis of these experiments, we propose that the main mechanism of action of PG-1 in lipid bilayers with physiologically relevant thickness as POPC lipids is toroidal pore formation. In this model, the peptide and lipids form supramolecular complexes shaped like toroidal pores (*2*, *10*). The lipid bilayer in the pore region bends back on itself, thus connecting the two leaflets of the bilayer. The resulting change in the lipid molecular orientation explains the loss of orientational order seen in the ^{2}H and ^{31}P spectra of POPC. Increasing the PG-1 concentration increases the number of such toroidal pores, eventually destroying the alignment of the glass plate samples. The high peptide concentrations at which the orientational order is abolished suggest that, in natural biological membranes, PG-1 may be highly aggregated to induce maximal damage. The fragmented lipid disks can be seen as the complementary part of the membrane to the toroidal pores: the former emphasize those lipids far away from the pores and unaffected by the peptides, while the latter describe regions of the membrane occupied and perturbed by the peptides.

The tilted orientation of PG-1 found in the short-chain DLPC lipids is not necessarily the peptide structure in the toroidal pores of POPC bilayers. The exact PG-1 orientation in POPC lipids is not yet determined due to the poor mechanical alignment. It is possible that PG-1 may also be tilted in POPC lipids. If this is true, its function may be as much to stabilize the lipids in the pore as to satisfy the hydrophobic matching. Investigation of the PG-1 orientation directly in long-chain phosphatidylcholine is in progress. In addition to the orientation aspect, one may speculate that PG-1 may self-associate to stabilize these toroidal pores. A recent solution NMR study of PG-1 in dodecylphosphocholine micelles indicates that the peptide forms antiparallel dimers and that several dimers may associate to form higher order aggregates (*46*). Such an aggregation may also exist in lipid bilayers and needs to be tested by independent experiments. Note that peptide aggregation would not affect the orientation measurements. In fact, the reduction of the number of non-hydrogen-bonded groups by intermolecular association should stabilize the interaction of the β-sheet peptide with the hydrophobic part of the lipids.

The present NMR evidence for the toroidal model as the mechanism of action of PG-1 is consistent with neutron and X-ray diffraction results and oriented circular dichroism results on PG-1 and magainin (*10*, *61*, *62*). The dramatic

change in lipid orientation and headgroup conformation at P/L greater than 1:30 also echoes the conclusion by Huang and co-workers that, above a threshold P/L value, magainin and PG-1 adopt different structures from the low-concentration state (*63*).

While the present study of the interaction between PG-1 and lipid bilayers used phosphocholine lipids, similar studies can be carried out in other lipids such as phosphatidylglycerol to understand the dependence of PG-1−lipid interaction on membrane composition. Efforts along these lines are currently in progress.

REFERENCES

1. Hancock, R. E., and Lehrer, R. (1998) *Trends Biotechnol. 16*, 82−88.
2. Matsuzaki, K. (1998) *Biochim. Biophys. Acta 1376*, 391−400.
3. Schibli, D. J., Hwang, P. M., and Vogel, H. J. (1999) *Biochemistry 38*, 16749−16755.
4. Wade, D., Boman, A., Wahlin, B., Drain, D. M., Andreu, D., Boman, H. G., and Merrifield, R. B. (1990) *Proc. Natl. Acad. Sci. U.S.A. 87*, 4761−4765.
5. Merrifield, R. B., Merrifield, E. L., Juvvadi, P., Andreu, D., and Boman, H. G. (1994) *Ciba Found. Symp. 186*, 5−20.
6. Bechinger, B. (1999) *Biochim. Biophys. Acta 1462*, 157−183.
7. Duclohier, H., and Wroblewski, H. (2001) *J. Membr. Biol. 184*, 1−12.
8. He, K., Ludtke, S. J., Heller, W. T., and Huang, H. W. (1996) *Biophys. J. 71*, 2669−2679.
9. He, K., Ludtke, S. J., Huang, H. W., and Worcester, D. L. (1995) *Biochemistry 34*, 15614−15618.
10. Ludtke, S. J., He, K., Heller, W. T., Harroun, T. A., Yang, L., and Huang, H. W. (1996) *Biochemistry 35*, 13723−13728.
11. Pouny, Y., Rapaport, D., Mor, A., Nicolas, P., and Shai, Y. (1992) *Biochemistry 31*, 12416−12423.
12. Bechinger, B., Zasloff, M., and Opella, S. J. (1993) *Protein Sci. 2*, 2077−2084.
13. Bechinger, B., Zasloff, M., and Opella, S. J. (1998) *Biophys. J. 74*, 981−987.
14. Marassi, F. M., Opella, S. J., Juvvadi, P., and Merrifield, R. B. (1999) *Biophys. J. 77*, 3152−3155.
15. Matsuzaki, K., Murase, O., Tokuda, H., Funakoshi, S., N, N. F., and Miyajima, K. (1994) *Biochemistry 33*, 3342−3349.
16. Salgado, J., Grage, S. L., Kondejewski, L. H., Hodges, R. S., McElhaney, R. N., and Ulrich, A. S. (2001) *J. Biomol. NMR 21*, 191−208.
17. Hill, C. P., Yee, J., Selsted, M. E., and Eisenberg, D. (1991) *Science 251*, 1481−1485.
18. Kokryakov, V. N., Harwig, S. S., Panyutich, E. A., Shevchenko, A. A., Aleshina, G. M., Shamova, O. V., Korneva, H. A., and Lehrer, R. I. (1993) *FEBS Lett. 327*, 231−236.
19. Steinberg, D. A., Hurst, M. A., Fujii, C. A., Kung, A. H. C., Ho, J. F., Cheng, F. C., Loury, D. J., and Fiddes, J. C. (1997) *Antimicrob. Agents Chemother. 41*, 1738−1742.
20. Tamamura, H., Murakami, T., Horiuchi, S., Sugihara, K., Otaka, A., Takada, W., Ibuka, T., Waki, M., Yamamoto, N., and Fujii, N. (1995) *Chem. Pharm. Bull. 43*, 853−858.
21. Nakashima, H., Masuda, M., Murakami, T., Koyanagi, Y., Matsumoto, A., Fujii, N., and Yamamoto, N. (1992) *Antimicrob. Agents Chemother. 36*, 1249−1255.
22. Chen, J., Falla, T. J., Liu, H., Hurst, M. A., Fujii, C. A., Mosca, D. A., Embree, J. R., Loury, D. J., Radel, P. A., Chang, C. C., Gu, L., and Fiddes, J. C. (2000) *Biopolymers 55*, 88−98.
23. Fahrner, R. L., Dieckmann, T., Harwig, S. S., Lehrer, R. I., Eisenberg, D., and Feigon, J. (1996) *Chem. Biol. 3*, 543−550.
24. Aumelas, A., Mangoni, M., Roumestand, C., Chiche, L., Despaux, E., Grassy, G., Calas, B., and Chavanieu, A. (1996) *Eur. J. Biochem. 237*, 575−583.
25. Cross, T. A. (1997) *Methods Enzymol. 289*, 672−696.
26. Antzutkin, O. N., Balbach, J. J., Leapman, R. D., Rizzo, N. W., Reed, J., and Tycko, R. (2000) *Proc. Natl. Acad. Sci. U.S.A. 97*, 13045−13050.
27. Long, J. R., Shaw, W. J., Stayton, P. S., and Drobny, G. P. (2001) *Biochemistry 40*, 15451−15455.
28. Yang, J., Gabrys, C. M., and Weliky, D. P. (2001) *Biochemistry 40*, 8126−8137.
29. Fields, C. G., Lloyd, D. H., Macdonald, R. L., Ottenson, K. M., and Nobel, R. L. (1991) *Pept. Res. 4*, 95−101.
30. Harwig, S. S., Waring, A., Yang, H. J., Cho, Y., Tan, L., and Lehrer, R. I. (1996) *Eur. J. Biochem. 240*, 352−357.
31. Rand, R. P., and Arsegian, V. A. (1989) *Biochim. Biophys. Acta 988*, 351−376.
32. Marra, J., and Israelachvili, J. (1985) *Biochemistry 24*, 4608−4618.
33. Yamaguchi, S., Huster, D., Waring, A., Lehrer, R. I., Tack, B. F., Kearney, W., and Hong, M. (2001) *Biophys. J. 81*, 2203−2214.
34. Hartzell, C. J., Whitfeld, M., Oas, T. G., and Drobny, G. P. (1987) *J. Am. Chem. Soc. 109*, 5966−5969.
35. Wu, C. H., Ramamoorthy, A., Gierasch, L. M., and Opella, S. J. (1995) *J. Am. Chem. Soc. 117*, 6148−6149.
36. Oas, T. G., Hartzell, C. J., Dahlquist, F. W., and Drobny, G. P. (1987) *J. Am. Chem. Soc. 109*, 5962−5966.
37. Hong, M., Gross, J. D., Hu, W., and Griffin, R. G. (1998) *J. Magn. Reson. 135*, 169−177.
38. Seelig, A., and Seelig, J. (1974) *Biochemistry 13*, 4839.
39. Huster, D., Yao, X., Jakes, K., and Hong, M. (2002) *Biochim. Biophys. Acta* (in press).
40. Gally, H., Niederberger, W., and Seelig, J. (1975) *Biochemistry 14*, 3647−3652.
41. Hong, M., Yao, X. L., Jakes, K., and Huster, D. (2002) (submitted for publication).
42. Lehninger, A. L., Nelson, D. L., and Cox, M. M. (1993) *Principles of Biochemistry*, Worth Publishers, New York.
43. Hartzell, C. J., Pratum, T. K., and Drobny, G. (1987) *J. Chem. Phys. 87*, 4324−4331.
44. Duncan, T. M. (1997) *Chemical Shift Tensors*, Farragut Press, Madison, WI.
45. Veeman, W. S. (1984) *Prog. NMR Spectrosc. 16*, 193−235.
46. Roumestand, C., Louis, V., Aumelas, A., Grassy, G., Calas, B., and Chavanieu, A. (1998) *FEBS Lett. 421*, 263−267.
47. Gennis, R. B. (1989) *Biomembranes: Molecular Structure and Function*, Springer, New York.
48. Seelig, J. (1978) *Biochim. Biophys. Acta 515*, 105−140.
49. Smith, I. C. P., and Ekiel, I. H. (1984) *Phosphorous-31 NMR: Principles and Applications*.
50. Thayer, A. M., and Kohler, S. J. (1981) *Biochemistry 20*, 6831.
51. Hong, M., Schmidt-Rohr, K., and Zimmermann, H. (1996) *Biochemistry 35*, 8335−8341.
52. Schmidt-Rohr, K., and Hong, M. (1996) *J. Phys. Chem. 100*, 3861−3866.
53. Hong, M., Schmidt-Rohr, K., and Nanz, D. (1995) *Biophys. J. 69*, 1939−1950.
54. Seelig, J., Macdonald, P. M., and Scherer, P. G. (1987) *Biochemistry 26*, 7535−7541.
55. Akutsu, H., and Seelig, J. (1981) *Biochemistry 20*, 7366−7373.
56. MacDonald, P. M., Leisen, J., and Marassi, F. M. (1991) *Biochemistry 30*, 3558−3566.
57. Altenbach, C., and Seelig, J. (1984) *Biochemistry 23*, 3913−3920.
58. deKroon, A. I. P. M., Killian, J. A., deGier, J., and deKruijff, B. (1991) *Biochemistry 30*, 1155−1162.
59. Roux, M., Neumann, J. H., Hodges, R. S., Devauz, P. F., and Bloom, M. (1989) *Biochemistry 28*, 2313−2321.
60. Pabst, G., Rappolt, M., Amenitsch, H., and Laggner, P. (2000) *Phys. Rev. E 62*, 4000−4009.
61. Yang, L., Weiss, T. M., Lehrer, R. I., and Huang, H. W. (2000) *Biophys. J. 79*, 2002−2009.
62. Heller, W. T., Waring, A. J., Lehrer, R. I., Harroun, T. A., Weiss, T. M., Yang, L., and Huang, H. W. (2000) *Biochemistry 39*, 139−145.
63. Huang, H. W. (2000) *Biochemistry 39*, 8347−8352.

BI0257991